ELSEVIER

Ultrasound in Med. & Biol., Vol. 23, No. 8, pp. 1209–1224, 1997

0301-5629/97 $17.00 + .00

PII S0301-5629(97)00123-3

● *Original Contribution*

THREE-DIMENSIONAL FREEHAND ULTRASOUND: IMAGE RECONSTRUCTION AND VOLUME ANALYSIS

C. D. BARRY, C. P. ALLOTT, N. W. JOHN,† P. M. MELLOR, P. A. ARUNDEL, D. S. THOMSON AND J. C. WATERTON

Departments of Cardiovascular and Musculoskeletal Research and Lead Discovery, Zeneca Pharmaceuticals, Alderley Park, Macclesfield, Cheshire SK10 4TG UK

(*Received* 17 *February* 1997; *in final form* 17 *June* 1997)

Abstract—A system is described that rapidly produces a regular 3-dimensional (3-D) data block suitable for processing by conventional image analysis and volume measurement software. The system uses electromagnetic spatial location of 2-dimensional (2-D) freehand-scanned ultrasound B-mode images, custom-built signal-conditioning hardware, UNIX-based computer processing and an efficient 3-D reconstruction algorithm. Utilisation of images from multiple angles of insonation, "compounding," reduces speckle contrast, improves structure coherence within the reconstructed grey-scale image and enhances the ability to detect structure boundaries and to segment and quantify features. Volume measurements using a series of water-filled latex and cylindrical foam rubber phantoms with volumes down to 0.7 mL show that a high degree of accuracy, precision and reproducibility can be obtained. Extension of the technique to handle *in vivo* data sets by allowing physiological criteria to be taken into account in selecting the images used for reconstruction is also illustrated. © 1997 World Federation for Ultrasound in Medicine & Biology.

Key Words: **Three-dimensional ultrasound, Free-hand image registration, Compound data reconstruction, Grey-scale segmentation, Volume measurement.**

INTRODUCTION

Our goal has been to develop a system based on freehand 2-D ultrasound scanning, capable of delivering precise and rapid 3-D reconstruction and leading to successful grey-scale segmentation and volumetric analysis. This system must also be capable of fitting into the biomedical and clinical research environments to allow 3-D ultrasound to take its place alongside the other mainstream imaging modalities of magnetic resonance imaging (MRI) and computerised tomography (CT) that can routinely exploit the advantages of 3-D imaging and analysis.

The value of 3-dimensional imaging has been well recognised for many years. Accurate sequential monitoring of pathology and other variables related to volume become possible, and meaningful structural information may be more readily communicated. The implementation of 3-D techniques to ultrasound has, however, proved to be a difficult and lengthy process. As early as 1956, 3-dimensional and stereoscopic observations were made on body structures by ultrasound (Howry et al. 1956). Reconstruction of ultrasound data in 3-D, allowing volumes to be measured independently of the data acquisition views and angles, was reported in 1980 (Moritz et al. 1980).

Since then, a considerable number of reports have appeared on the development of methods for 3-D reconstruction of ultrasound data (for reviews, see Vogel et al. 1995; Rankin et al. 1993; Levine et al. 1992). Several studies describe methods using conventional 2-D transducers to acquire parallel or near-parallel image sets. The transducer may be advanced with a stepping motor (Franceschi et al. 1992; Hell 1995; Moskalik et al. 1995; Vogel et al. 1995), by a freehand sweep (Geiser et al. 1982; Gardener et al. 1991; Kelly et al. 1994; King et al. 1990; Moritz et al. 1980; Nelson et al. 1996; Riccabona et al. 1995) or, in intravascular studies, by timed pullback of the catheter (von Birgelen et al. 1995; Mintz et al. 1992; Rosenfield et al. 1991), or by rotation about a central axis (Kok-Hwee et al. 1994).

† N. W. John's present address is: Silicon Graphics Computer Systems, Laser House, Waterfront Quay, Salford Quays, Manchester M5 2XW UK.

Address correspondence to: Dr. C. D. Barry, Zeneca Pharmaceuticals, Alderley Park, Macclesfield, Cheshire SK10 4TG, UK.

Where freehand techniques are used, the image positioning can be obtained from simultaneous recording of the position and orientation of the transducer using mechanical arm, acoustic spark gap or electromagnetic sensor techniques (Detmer et al. 1994; Geiser et al. 1982; Gardener et al. 1991; Hernandez et al. 1996; Kelly et al. 1994; King et al. 1990; Moritz et al. 1980; Moskalik et al. 1995; Nelson et al. 1996; Riccabona et al. 1995).

Dedicated 3-D ultrasound systems that utilise tomographic transducers to interrogate a volume by either internal mechanical sweeping techniques or by use of a 2-D array have also been described (Hamper et al. 1994; von Ramm et al. 1994; Zosmer et al. 1996).

To date, all the methods that have been described for 3-D ultrasonography have limitations. Described systems based on stepping motors or freehand sweeps have been limited by the relatively low number of data slices contributing to the 3-D reconstruction, or the large slice interval. Data interpolation techniques have been used to "fill in" the missing data for reconstruction. Coincident image frames have been actively avoided to overcome the problem of dealing with multiple values being generated for a single point in the data block. As has already been pointed out in the literature (Nelson et al. 1996), this prohibits any possibility of compounding data to improve the quality of the 3-D images. Dedicated 3-D transducers are often bulky and can only be used to acquire a 3-D volume equal to the insonated volume from a stationary probe. Such systems may limit the ability to obtain preferred views, particularly where shadowing may occur from overlying structures. Insonation angle for data acquisition is often fixed in the 3-D methods, but 2-D ultrasonography routinely allows interrogation from a variety of angles to optimise structure boundary definition. The angle dependency of ultrasound reflection and backscatter intensities when investigating tissue composition were reported in 1985 (Picano et al. 1985). An ability to "compound" these multiple angles of insonation into a single data set would significantly improve signal-to-noise and, thus, speckle contrast and produce the most coherent object for segmentation and reconstruction (Hernandez et al. 1996; Hughes et al. 1996; Moskalik et al. 1995; Nelson et al. 1996; Shattuck and von Ramm 1982).

Satisfactory 3-D reconstruction from freehand 2-D ultrasound images requires precise spatial registration of the ultrasound image in a common reference frame. Compounding of the data places a particular emphasis on the precision of this registration and requires compensation for systematic errors associated with any position-sensing device (Detmer et al. 1994; Moskalik et al. 1995). A 3-D data block can then be generated and the intensity data from each image extracted into its appropriate position. A precise method of compensating for, or gating to, physiological motion, such as the cardiac pressure cycles in blood vessels using electrocardiographic (ECG) recording, is often essential to ensure that such motion does not disrupt or deform the integrity of the structure to be reconstructed. Also, if the technique is to have any practical application, the output from the process must be available within a short time of completing the scan and be in a form that can exploit the highly efficient image processing and analysis tools developed for other medical imaging modalities. Although computer model-fitting to generate volume measurement could be used, this may not deal adequately with pathology. A sufficiently high degree of confidence and reliability in the results of automated segmentation on the basis of reconstructed, grey-scale, echo intensities and any subsequent volume measurements and analysis require the generated 3-D ultrasound image quality to be improved beyond that represented by a typical 2-D ultrasound frame.

Thus, in our view, the optimal 3-D ultrasound system requires that:

- The ultrasound scanning equipment is not irretrievably modified.
- The freehand, interactive nature of ultrasound scanning be maintained as near normal as possible with the option for 2-D analysis retained.
- All data be recorded continuously rather than restrict acquisition to particular periods within the cardiac or respiratory cycles. Postprocessing techniques can then be used to select appropriate image frames. This allows reinterrogation of data at different physiological states without the need to repeat the ultrasound scan.
- The intensity values in the 2-D ultrasound images be preserved to allow reconstruction, volume measurement and grey-scale analysis of the acquired data.
- Image quality be improved beyond that represented by typical 2-D ultrasound.
- A 3-D data block be generated, directly compatible with 3-D image analysis software products.

In this paper, we describe a system that is capable of fulfilling these criteria, delivering significant benefits at no risk to the equipment or the ability to revert to conventional 2-D analysis of the ultrasound images.

METHODS

System implementation

The system implementation falls into 3 separate phases (Fig. 1):

- Data acquisition to S-VHS video tape
- Data extraction and 3-D reconstruction
- Analysis and presentation of 3-D reconstructions.

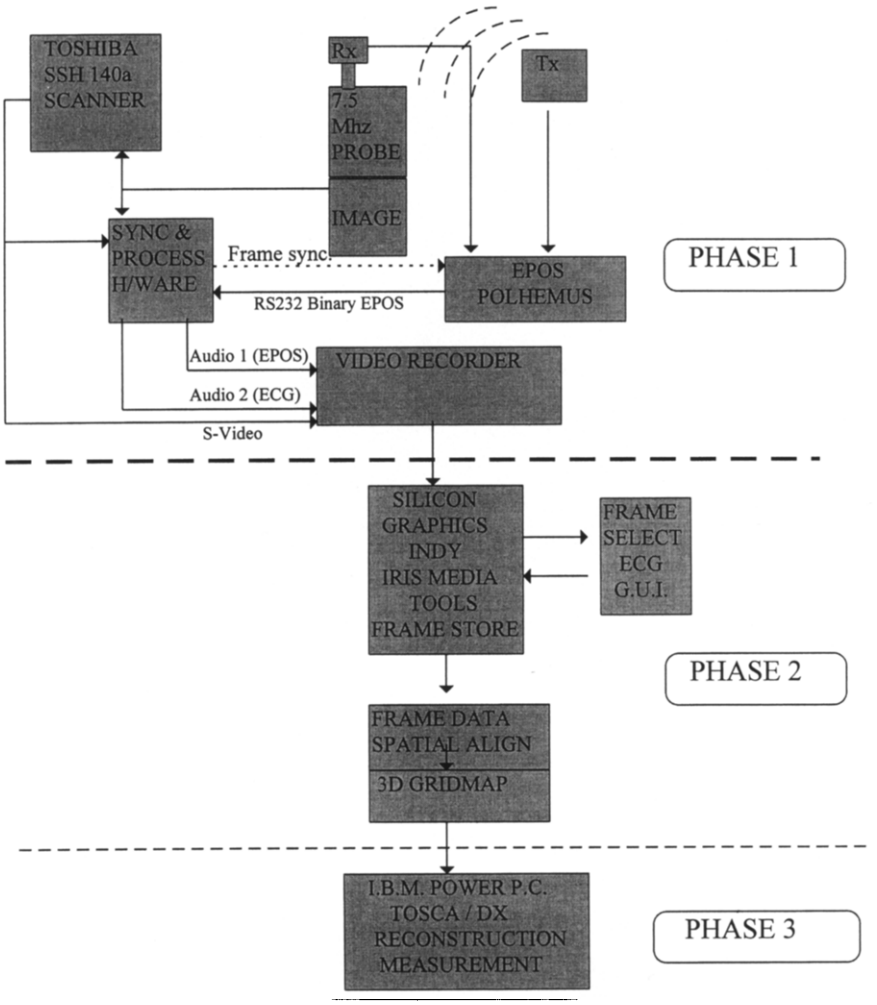

Fig. 1. Diagram of 3-D freehand ultrasound system components.

Data acquisition to S-VHS video tape

Phase 1 comprises the complete and continuous recording of the ultrasound images, their encoded positional information and any ECG wave form. The 3 inputs were captured on the video and 2 associated stereo audio channels of an S-VHS video recorder (Panasonic AG 7350, Matsushita Electric Industrial Co., Ltd., Osaka, Japan). The ultrasound image frames were generated on a Toshiba SSH 140a ultrasound scanner (Toshiba Medical Systems UK, Crawley, UK) fitted with a 7.5 MHz linear array transducer. The positional information for registration was obtained from an electromagnetic position and orientation sensor (EPOS) Polhemus 3 Space Isotrak II system (Polhemus Inc., Colchester, VT), controlled and synchronised by custom hardware developed at Zeneca. This customised hardware also conditioned any ECG signal to a format suitable for recording on the video audio channel.

Acquisition of ultrasound images to tape. All ultrasound scans were performed using a Toshiba SSH 140a ultrasound scanner fitted with a 7.5 MHz linear array transducer. Image generation parameters were preset to optimise the visualisation of the object of interest. B-mode ultrasound images were acquired at the standard rate of 31 frames per second (fps) and, during interrogation, were recorded continuously using an S-VHS PAL video recorder (Panasonic) at the lower rate of 25 fps, the remaining 6 fps being dropped systematically during video readout from the internal frame buffer of the scanner: a single interrogation generating around 10,000 2-D images on videotape.

Signal-processing hardware. Custom-built, modular, signal-processing hardware was developed at Zeneca to allow the recording of positional and any ECG information onto the 2 hi-fi audio channels of the video recorder.

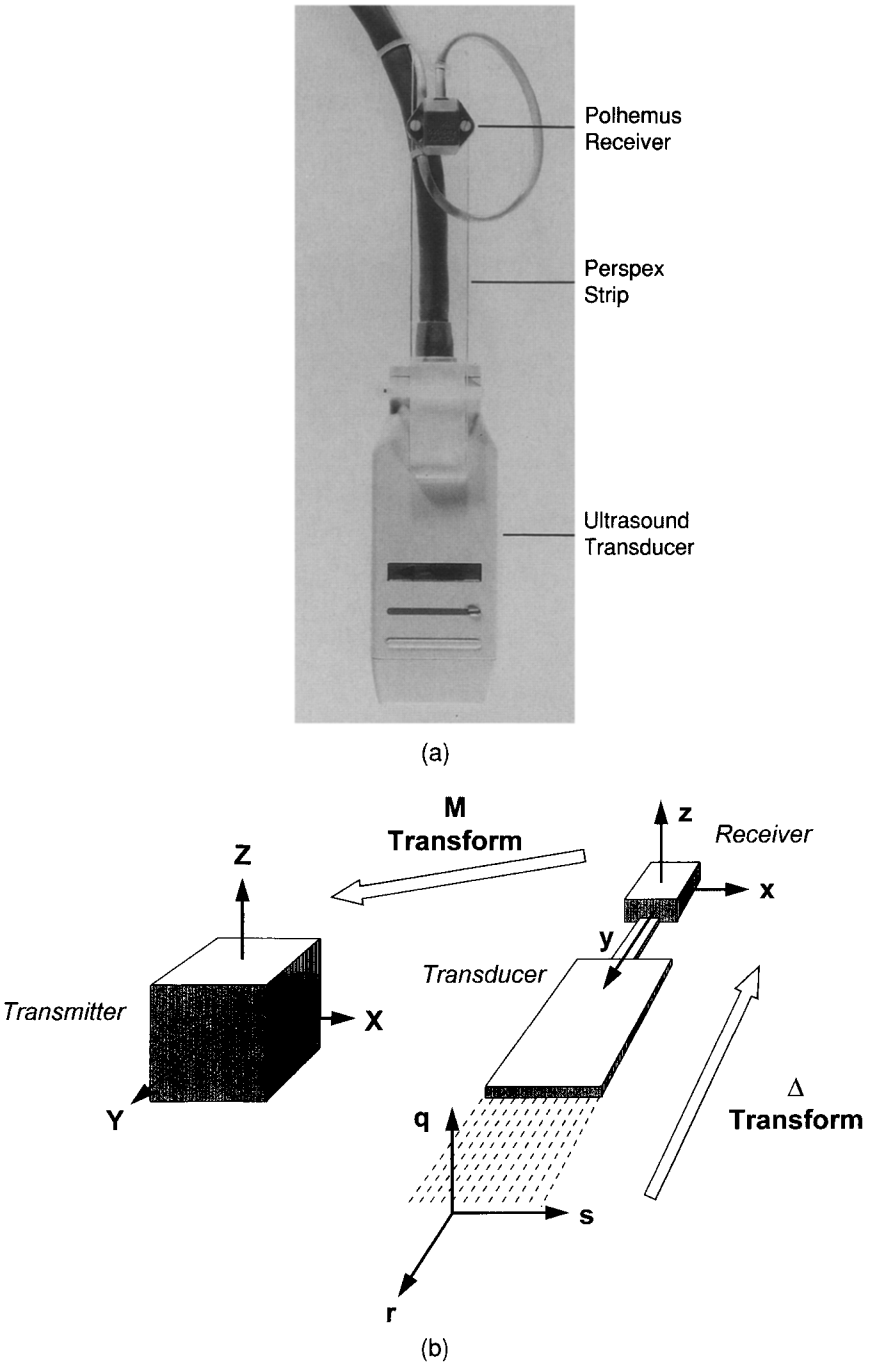

Fig. 2. (a) Photograph of the physical arrangement of ultrasound transducer and Polhemus EPOS receiver. (b) Coordinate systems and transformations for 3-D spatial location of 2-D ultrasound images.

Recording the positional information. Ultrasound transducer positional information was obtained from an electromagnetic position and orientation sensor (EPOS), Polhemus 3 Space Isotrak II, attached to the ultrasound scanning transducer as shown in Fig. 2a.

The first process module generated the required command line for the EPOS by a programmable controller (PIC16C54), following a single manual contact closure. The controller was clocked by an 8 MHz crystal oscillator, communicating with the EPOS *via* an RS-232 line driver (MAX233) that operates at 9600 baud. The command line consisted of 13 characters defining the output list as the *x, y, z* linear coordinates, plus angles for roll, pitch and yaw, interspersed with "carriage return"

and "line-feed" commands. On receipt of a synchronising pulse (see below), the EPOS transmitted the output list corresponding to the sensor position at that instant and, therefore, corresponding to the current video frame. This output binary data stream was returned to the module and scaled, using a line driver (MAX483) and potential divider, to provide a 0.4 V amplitude unbalanced signal suitable for the audio input channel of the S-VHS video tape recorder.

For each video frame to be recorded together with the corresponding positional information, synchronisation was necessary between the scanner and EPOS. The latter was run in "noncontinuous" mode, awaiting a pulse to start the data stream. To achieve this, the composite video output from the scanner was taken to a purpose-designed "synchronisation " module. The composite signal was fed to a sync separator circuit (TDA8128) that provided an output pulse for each video field. Because 2 interlaced fields form each frame, a bistable circuit (4013) was used as a divide-by-2 to give a single output pulse per frame. This monophasic pulse activated a differential line driver (MAX483) to provide the external synchronisation signal for the EPOS. A simple diode-pump circuit also integrated field pulses to light an indicator as a visual confirmation of synchronisation pulse presence.

The above processing was designed to ensure that the positional information was sent to the tape concurrently with the corresponding video frame. In practice, there was a slight latency of around 18 ms between the instant of frame starting and the positional data stream. This was accurately measured and compensated for during subsequent editing in the digital frame store medium.

ECG recording. In choosing to record ultrasound interrogations continuously and not utilise instrument gating, a facility has been provided to enable frames to be selected for reconstruction on the basis of their temporal position in the cardiac cycle in the case of *in vivo* interrogations. When necessary, a conditioned ECG signal is recorded on the second hi-fi audio channel of the video recorder.

The ECG conditioning module can be considered in two sections. The electrically isolated front end consisted of a conventional differential instrumentation preamplifier (Burr-Brown Ltd., Livingston, West Lothian, UK) with a voltage gain of 50, configured together with an external operational amplifier to provide active drive of the indifferent electrode. This front end was interfaced with the second section of the circuit *via* an isolation amplifier (Burr-Brown ISO 107) that also provided isolated power supplies for the preamplifier and driver. There was no ground connection to the subject, the resultant isolation (2500 volts a.c. rms, 3500 volts d.c.) allowing safe clinical use. The isolator output was connected, *via* a variable attenuator, to the second, nonisolated, section of the circuit. This consisted of a capacitively coupled inverting amplifier, with a fixed d.c. gain of $\times$ 10, and low-pass filtering to remove the high-frequency ripple artefact induced by the oscillator within the isolation amplifier. An output socket at this point provided amplified ECG for display on the ultrasound scanner screen by connection to the high level d.c., nonisolated, patient input socket. A second output of this ECG stage was routed within the module to a differentiator for enhancement of the QRS wave and partial suppression of the P and T waves. A fast time-constant removed baseline shifts. This heavily filtered version of the ECG was scaled for recording through a hi-fi audio channel (20 Hz to 20 kHz) on the S-VHS video tape recorder, and was stored concurrently with the video images.

Data extraction and 3-D reconstruction

Phase 2 starts with the transfer of a continuous sequence of image frames, each with its associated EPOS and ECG data, from the video tape to the computer. This is followed by the selection of a subset of frames on the basis of their image content and/or timing within the cardiac cycle and, finally, the reconstruction process.

Ultrasound image extraction. Data from the videotape were digitised on a 100 MHz silicon graphics Indy R4600PC workstation configured with 96 Mbytes of memory, a video option card, and a Cosmo Compress motion JPEG (Joint Photographic Experts Group) video compression card. Four external SCSI disks were connected to the Indy and striped to provide a fast 8 Gbyte disk store. To achieve real-time video acquisition with ultrasound images (using PAL timing), the JPEG quality factor on the Cosmo card was set to 75%, giving approximately 15:1 compression ratio. Data were stored in Silicon Graphics' proprietary movie file format. Typically, 4 min of video were acquired, providing movie files containing 6000 image frames and occupying 600 MBytes.

EPOS and ECG data extraction. The audio hi-fi channels containing the ECG and EPOS data were sampled using the Indy analogue audio input at 48 kHz. The audio files produced in Silicon Graphics format were linked to the Moviefile in such a way that the audio associated with any individual image frame could be uniquely extracted. The positional information and ECG could be then be carried and processed with any selected image frame.

Silicon Graphics' IRIS Digital Media software tools Audio Panel, Video Panel, and Capture, supplemented with software written in-house, provided a user interface

for all data capture. Review and selection of image and audio frames was provided by Movie Player, Movie Maker, and Sound Editor, again supplemented with software written in-house.

Image frame selection. For data sets where there was no cardiac-cycle motion associated with the structure under investigation, intact sequences of frames, or appropriate subsets, were selected and extracted using custom command-line utilities indicating start, end and frame interval.

Where ECG gating of images is required to eliminate motion associated with the cardiac cycle, this can be done retrospectively using the digitised QRS waveform. For this purpose, a utility has been developed with an easy-to-use graphic interface that allows frames to be selected based on their position within cardiac cycles whose duration falls within a specified range. Interrogation of the digitised audio channel containing the processed ECG waveform displays a histogram of cycle lengths from which the user selects the most relevant samples. The user specifies a time- or percentage-based window in the cardiac cycle for which frames will be selected, avoiding the use of excessively long or short duration cycles. For each valid ECG cycle, the exact time for the end-points of this window is calculated and mapped to the corresponding frames on the image track of the movie file to generate a "valid frames list" file.

Typically, about 500 valid frames will be selected from each data set for 3-D reconstruction and recorded in the "valid frames list" file.

Image frame processing. Some preliminary processing of the ultrasound video frames was undertaken. The data captured in 32-bit integer format by the Cosmo Compress card was reduced to 8-bit grey-scale values. Deinterlacing of the PAL video was provided, and redundant video information, such as text, grey-scale bar, blank spaces and grid lines were removed. Finally, to reduce further the sheer quantity of data to be processed by the 3-D reconstruction software, images were scaled to half their original size using a standard anamorphic image-scaling algorithm (Schumacher 1991). This preliminary processing achieved an overall reduction of about 98% in data size without compromising significantly the quality of the final reconstructions. Extraction from the movie file and conversion to the required format was performed by a background batch process controlled by customised command-line utilities and the previously generated "valid frames list" file. Using our 100 MHz, R4600-based SGI Indy, this task took approximately 3 s per image; however, this reduces very significantly using R5000- and R10000-based systems now available at a similar cost.

3-D registration of ultrasound image data. In our experimental system, the EPOS transmitter was sited at a convenient location within a 30 cm radius of the object being scanned and remained fixed throughout the data acquisition. The origin and axes of the transmitter established the fixed "registration frame" (designated XYZ in Fig. 2b). The EPOS readings tracked the position and orientation of the receiver and, thus, the receiver coordinate frame (designated xyz), relative to the fixed transmitter frame. The transformation relating the coordinates of a point in frame xyz to those of the same point in frame XYZ was designated M and obtained directly from the EPOS. The EPOS receiver was attached to the ultrasound transducer by securely mounting on a short (15 cm) plastic strip to minimise electromagnetic influences (Fig. 2a). The coordinate frame associated with the ultrasound image itself (designated qrs, with q always zero), although fixed relative to the receiver frame xyz, has an offset in both position and orientation. A transformation, including both translation and rotation, had to be applied to correct for the position and orientation of the EPOS receiver in relation to the 2-D ultrasound image. We refer to this as the Delta (Δ) transformation, which has to be determined only once for each specific mounting of the EPOS on the ultrasound transducer before the ultrasound images can be properly registered.

Specifically, the transformations M and Δ together relate the co-ordinates of a point in space measured using the ultrasound image axis system qrs to the coordinates of the same point measured in the registration axis system XYZ.

If the former coordinates are represented by *p(qrs)* and the latter by *P(XYZ)*, then:

$$\left.\begin{aligned} P(XYZ) &= M^{*}\Delta^{*}p(qrs) \\ \text{or}\quad p(qrs) &= (M^{*}\Delta)^{-1}{}^{*}P(XYZ) \\ &= \Delta^{-1}{}^{*}M^{-1}{}^{*}P(XYZ) \end{aligned}\right\} \qquad (1)$$

Determination of the delta transformation. The delta (Δ) transformation was determined by scanning a calibration phantom consisting of 2 crossed threads suspended in a bath of 20% w/v galactose solution using a wide range of transducer angles and positions. The galactose solution provided a transmission medium for the ultrasound that more closely corresponded to the speed of sound transmission in normal tissue than does water. The crossover provided a point in space whose coordinates were unknown but fixed in relation to the EPOS transmitter. After digitisation on the Silicon Graphics Indy, the frames containing images where the cross was visible were extracted from the movie file. These 2-D frames were displayed and the image location of the

centre of the cross (*r,s*) determined and noted. A minimum of 2 observations were made for each attitude, totalling some 50 observations of this unique point in space. The vastly overdetermined series of equations relating the unknown fixed position, *P(XYZ)* and transformation Δ to the known value pairings of *p(qrs)* and *M*, eqn (1) was then solved for *P(XYZ)* and Δ. Here, an iterative process was used based on a starting trial Δ followed by a steepest descent refinement of the 3 angles and 3 distances defining the transformation. The criteria function minimised was the root-mean-square deviation of the individual estimates of *P(XYZ)* from their group mean. The resulting Δ transformation matrix calibrated the specific ultrasound transducer/EPOS receiver configuration for fixed settings of the "field of view and scaling" parameters for the scanner. Any change in these 2 parameter settings, in general, will result in the introduction of a new "*qrs*" coordinate system and require experimental determination of the new Δ transformation matrix; a mathematical relationship will exist between any 2 such Δs that will be unique for the specific transducer.

The method has been extended to use independent sets of data corresponding to scans of either different point phantoms or the same phantom with different transmitter locations, combining these into a single, improved estimate. This is achieved by computing the rms measure of the criteria function for each set of data and using the sum of these as the refinement criteria. Further extension of this procedure to use a weighted sum allows incorporation of an assessment of the quality of the individual scans.

Eqn (1) has also be used as the basis of an alternative estimation of using the same point phantom approach. The group mean *P(XYZ)* was back-transformed and the coordinates of this point in the individual ultrasound image coordinate systems, *p(qrs)*, calculated. The difference between these back-transformed coordinates and their original, observed positions was used to compute the criteria function, with the option now of reducing the contribution (weighting) of the component perpendicular to the ultrasound image plane, *q*, relative to the better resolved in-plane components (*r* and *s*). A relative weighting of 1.0 reproduced the results of the original refinement procedures and a weight of zero typically produced a Δ differing by several degrees in orientation and millimetres in translation, being a highly significant change.

3-D reconstruction using grid-mapping. Determination of the Δ transformation calibrates the ultrasound transducer/EPOS configuration necessary for the accurate registration of the 2-D ultrasound images in the 3-D coordinate system established by the fixed transmitter. The second critical step is grid-mapping. This is the process that uses the data values observed on a number of oblique, nonparallel ultrasound planes to compute the echo intensities at points on a regular 3-D grid in a format compatible with software for presentation, segmentation and analysis. It is essential that the algorithm used for this application be very efficient because a typical reconstruction will involve the calculation of about 2 million new positional intensity values from an input data set of some 12 million values contained on 500 registered frames.

There are 2 possible implementations of this algorithm. The first involves sequencing through the regular array of grid positions and, at each point, identifying and using the subset of the US data that is "relevant" to the calculation of the grid value. The second involves sequencing through the input data points and accumulating the contributions to the "relevant" subset of grid positions. In both cases, the "relevant" subsets can be specified by introducing a limiting radius *R*, within which the relative weights of contributions are made a function of the distance *r* between the data point and the grid position.

Although the first option might appear the more direct, the second is, in fact, much more efficient. In addition to allowing full advantage to be taken of the systematic organisation of the US data, the second approach enables effective use to be made of the limiting radius to reduce very significantly the number of grid-point, data-point pairs used in the calculation of the 3-D reconstruction. In typical cases where the limiting radius *R* is of the same magnitude as the data spacing on the ultrasound frame and of the grid spacing (0.2 mm), the saving in computation time can approach the ratio of the volume of the grid-mapped box to the volume of a sphere of radius *R*.

Our implementation follows the second approach and uses an "inverse distance" weighting scheme with 2 nested cycles, the outer cycle indexing through the individual 2-D ultrasound frames, the inner cycle indexing through the data values and positions associated with each of the US frames. As the 2-D ultrasound frames are processed, 2 sums are accumulated for each voxel in the reconstruction. The terms of the first sum are the measured echo intensities of the ultrasound data points which, when registered in 3-D, fall within the limiting radius *R* of the voxel centre, scaled by a factor equal to the inverse distance from the voxel centre to the data point. The terms of the second sum are the inverse distance-scaling factors themselves. The ratio of the final values of these 2 sums provides the normalised, distance-weighted average assigned to the voxel.

The location and orientation of the 3-D reconstruction grid is defined in relation to a user-selected KEY

ultrasound frame, typically one that is centrally located and depicts a complete cross-section of the object of interest. The orientation and position of the KEY ultrasound frame relative to the EPOS transmitter coordinate system is determined by the EPOS values and knowledge of the Δ transformation. The origin of the 3-D grid will be at the centre of the KEY frame and the grid axes will be parallel to those of this ultrasound frame. The transformation relating the EPOS transmitter coordinate system and that of the 3-D reconstruction grid is obtained from the coordinates of the centre of the KEY frame and the normalised axis-vectors of the oriented KEY frame.

Analysis and presentation of reconstructions

Phase 3 of the system covers the segmentation, presentation and analysis of the information inherent in the reconstructed 3-D array of echo intensities.

Image analysis and measurement was provided by commercially available software from IBM: TOSCA (Tools for Segmentation, Correlation and Analysis) and DX (Data eXplorer) mounted on Power PC UNIX workstations configured with 128 Mbytes or more of memory, 3 Gbytes of disc, 80 MHz processor and GT4E graphics adapter. TOSCA implements a 3-dimensional region-growing algorithm for automatic grey-scale segmentation (Elliot et al. 1996; Sivewright and Elliot 1994). Using the statistics for the voxel values in the immediate neighbourhood of a user-selected seed-point that are characterised by window and level parameters, the algorithm tests adjacent voxels for inclusion in the same region-of-interest (ROI), iterating this process until there are no more contiguous voxels consistent with the seed-point statistics. For display purposes only, a smooth contour or surface is generated bounding the ROI; the volume is determined by counting the statistically acceptable voxels rather than by estimating the volume bounded by the smoothed surface. Such volume estimates compare well with results obtained using other methods based on contouring techniques or on edge detection algorithms, provided the boundary of the ROI is reasonably continuous and uniform in intensity.

System evaluation

The system was evaluated against 3 criteria, the ability to provide accurate estimates of volumes in the range encountered with atherosclerotic plaques and small tumours, the ability to improve overall image quality through carefully registered spatial compounding and, finally, the ability to carry out *in vivo* reconstructions of clinical relevance. The first 2 studies employed phantoms scanned at room temperature using galactose solutions to match the 1540 m/s sound velocity for tissue inherent in the scanner's internal calibration of image depth.

Phantom studies. The accuracy of reconstruction and volume measurement of the system was evaluated using a series of 3 water-filled balloon phantoms of volumes between 0.9 and 8.0 mL The phantoms were mounted in a bath of 20% w/v galactose solution and each scanned using the system described, employing several free-hand sweeps to explore a wide variety of insonation angles. After 3-D reconstruction, the volumes were measured 3 times using the automatic grey-scale segmentation and analysis tools in TOSCA, relying entirely on the integrity of boundaries produced by the system described. After measurement, the latex balloons were dried and weighed. The balloons were then punctured, dried and reweighed. The volume of distilled water contained within the balloon was obtained from the weight difference, assuming a density value at room temperature (22°C) of 0.9978 g/mL.

A second series of phantoms was used to introduce internal structure and texture, as well as provide volumes of different shape. These phantoms were cylinders cut from a block of foam rubber by cork borers of known diameters, then trimmed to length providing volumes of approximately 0.75, 1.00 and 2.50 mL. The phantoms were again scanned in a bath of 20% w/v galactose solution. Measurements of the "wet" cross-sectional diameters and cylinder length were made from the 2-D ultrasound images for volume calculation. A more direct estimation of volume by displacement was not possible here because the integrity of cells in the foam could not be guaranteed. As a consequence, each cylinder length and diameter was measured in 3 positions on each scan; the mean values from these observations being used to calculate "best estimated volume." This was compared to the 3-D volume, again measured in TOSCA by volume-growing algorithms based on segmentation of the 3-D data block at preset level and window. The level and window were chosen by displaying a profile of the intensity values across the object within the data block, then selecting a mean value for level and an appropriate window to delineate the edges of the object. Two observers measured each data set with their own preferred level and window. The 2 data sets on each phantom were processed independently in an attempt to evaluate the reproducibility and objectivity of volume measurement by this method.

Image quality studies. The effect of grid-mapping high-density sampled data acquired with multiple angles of insonation was investigated by 2-D image comparison. One image was the "key frame" taken directly from the ultrasound acquisition video and the other was the central plane of the grid-mapped 3-D data set. This reconstructed plane was identical in position and orientation with the input "key frame" and representative of

the quality of all reconstructed planes at this data density. For the results to be meaningful, it was important in these studies that the boundary of the ROI was well defined. The foam-rubber phantom described above was chosen to provide a high contrast interface with the galactose bath and a high degree of uniformity in the echogenicity of boundary.

Statistical analysis of these images and the contributing data provided the mean pixel value for the whole image, the number of 2-D ultrasound data values contributing to each grid point, and the percent coefficient of variation (% CoV) of the weighted contributions to the computed mean pixel value. These characterise the quality of individual pixel values. The % CoV serves as the ultrasound analogue of the noise-to-signal ratio encountered with other imaging modalities and is, thus, a direct measure of speckle contrast (Hernandez et al. 1996). There is also a need to characterise the ability of statistical segmentation tools to generate a volume of interest (VOI) on the basis of grey-scale intensities. This involves considering the "coherence" of the intensities of the pixels forming the boundary of the VOI, as defined below.

A simple measure of coherence was obtained by examining the number of pixels identified in the interface boundary at a fixed level (40) and window (2), and the variation of intensity of the pixels along the boundary in the IBM DX environment. The "segmentation window width" required to produce a continuous boundary at a fixed level (40) provided a similar, but independent, measure of the inverse of this coherence.

A more automatic and tool-independent measure has been implemented by applying a 3 × 3 inverse distance filter (F) at each pixel location in the 2-D image plane.

$$F = \frac{1}{6.8} \cdot \begin{pmatrix} -0.7 & -1.0 & -0.7 \\ -1.0 & 6.8 & -1.0 \\ -0.7 & -1.0 & -0.7 \end{pmatrix} \qquad (2)$$

The filter result for each pixel in the image was then normalised by the original pixel value and the absolute value of the result expressed as a percentage. These percentage values can be used to colour-code a display to reveal areas of high or low coherence within a region of interest, greater coherence again represented by the lower percentage values. The average of these percentage values taken over a region offers an over-all coherence measure. Specifically, we define a "Coherence Number" for the reconstructed map or an individual plane that is equal to 100 divided by the mean of the percentage values for the map or plane.

Human carotid reconstructions in vivo

To illustrate potential clinical applications for the techniques described, 3-D data sets were produced from *in vivo* carotid scans using two of the authors as subjects. These scans were taken predominantly in the transverse (XY) plane and the accompanying ECG traces were used to select the 2-D ultrasound frames for inclusion in the reconstructions. The 3-D data sets were segmented and then surface rendered to show the topology of the vessel-lumen boundary. In addition, two orthogonal planes were extracted through the centre of the data block; one was parallel to the general scanning direction (XY), the other perpendicular (XZ). The latter represents a longitudinal view virtually unobtainable as part of a conventional scan due to the anatomical constraints on the positioning of the ultrasound probe.

RESULTS

Reconstructions

After processing, all data sets were reconstructed and displayed, processing usually taking less than 30 min, including batch processing time. The regular shapes of the phantoms allowed visual assessment of the reconstructions regarding distortions or disruptions of shape; no obvious distortions or disruptions of shape were discerned and even the 0.5 mm wire used to suspend the foam-rubber phantoms was successfully resolved (Fig. 3).

The spatial resolution of the system as implemented has a theoretical isotropic limit of 0.2 mm from the anamorphic scaling to half size of 2-D ultrasound images with an in-plane resolution of 0.1 mm. The out-of-plane resolution of the 2-D images is controlled by the beam-thickness profile of the transducer and is on the order of 1 mm, even at the focal depth. Without the use of the multiple insonation angle, spatial-compounding technique, this much larger value would dominate the spatial-resolution characteristics and render them very significantly anisotropic. The degree to which the system's spatial resolution approaches the theoretical limit will, instead, depend on the extent of the compounding (number of ultrasound planes and diversity of insonation angle) and on the quality of the Δ matrix used in image registration. On the basis of the statistics related to the Δ matrix determination using the cross-wire phantom, the spatial resolution of the system was determined to be 0.5 mm isotropic. This figure had an associated standard deviation of 0.18 mm and was consistent with the quality of the results and images presented throughout the paper.

Accuracy of volume determination

Volume measurement from the balloon phantoms was straightforward, in that the grey-scale segmentation

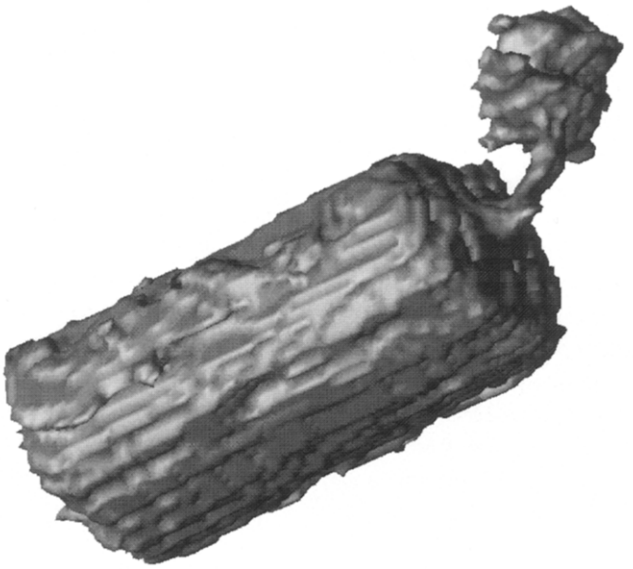

Fig. 3. Surface-rendered 3-D reconstruction of a 700 mm^3 foam-rubber cylinder and 0.5-mm diameter supporting wire used as a phantom for the reported studies.

tools within TOSCA were able to detect the internal surface of the balloon. Grey-scale segmentation within this surface provided reproducible volumes with rms accuracy of 1.1% (Table 1).

Best estimated volume of the foam cylinders was calculated from the mean diameter and length measurement by:

$$\text{Vol} = \pi\left(\frac{d}{2}\right)^2 \cdot L \qquad (3)$$

where d = mean diameter of the cylinder and L = mean length. Overall mean values for volumes were obtained for precision determination, and individual operator values for volumes from both independent data sets on each phantom for reproducibility (Table 2).

Three measurements of the 2 data sets from each of the foam phantoms, by 2 independent observers, resulted in good overall reproducibility. Observer 1 demonstrated a CoV of between 5% and 2% for the model-based calculation of volumes compared to an overall 1% CoV for 3-D analysis. Observer 2 demonstrated a 2% CoV for the model-based volume measurement against a 1% CoV for 3-D analysis. Overall precision of 3-D measurement is illustrated by an rms coefficient of variation of 1.4% (test-retest) and 1.3% (inter-observer).

Comparative measures of image quality

In all cases the "compounded" grid-mapped reconstructions offer very significant improvements in interface coherence and, hence, the ability to segment volumes of interest based on intensity values. By using: 1. The foam-rubber phantom to provide high contrast in-

Table 1. Accuracy of balloon phantom volume measurements.

	Actual weight of water (g)	Calculated volume (0.9978 g/mL)	Volumes from 3D ultrasound (mL)
Balloon 1	0.90	0.90	0.89
			0.89
			0.88
Balloon 2	4.65	4.66	4.64
			4.68
			4.67
Balloon 3	7.92	7.94	7.84
			7.84
			7.83

Table 2. Precision of foam phantom volume measurements.

		Volume estimated from 2D slices (cylindrical model) μl ± SD	Volume measured from 3D ultrasound (model-free) μl ± SD	
			First scan	Repeat scan
Phantom 1	Observer1	699 ± 19	709 ± 10	703 ± 4
	Observer2	717 ± 34	719 ± 0	694 ± 20
Phantom 2	Observer1	956 ± 8	967 ± 9	971 ± 12
	Observer2	975 ± 10	985 ± 5	986 ± 1
Phantom 3	Observer1	2405 ± 13	2356 ± 10	2325 ± 23
	Observer2	2398 ± 42	2339 ± 0	2401 ± 33

Table 3. Statistical properties of 2D ultrasound image and reconstructed image plane.

Attribute	2D Ultrasound frame	Plane from typical reconstruction†
Compounded	No	Yes
Insonation angle ranges	Single fixed angles	Azimuth: 83° Elevation: 30° Roll: 130°
Average number of data points per grid point	1	66
% CoV of weighted pixel mean (frame/plane average)	Single value only, no statistics	0.23%
Boundary continuity measures		
Segmentation window width	8.5	2.9
Number of pixels identified (345 max)	121	293
Coherence number	51	195

†500 frames with R = 0.25 mm.

terfaces with a relative uniform boundary density, and 2. positioning the 3-D grid using the KEY 2-D plane so that direct comparison of a "raw" vs. a reconstructed data plane can be made, it has been possible to quantify the improvements in image quality that can be achieved with reconstructions based on compounded, free-hand scanned, high-density sampled data sets (Table 3, Fig. 4a and b).

The extent to which compounding was used in the reconstruction is shown by the range of angles and the average number of ultrasound data points used in calculating each value in the reconstructed central plane. This average increased with both the number of ultrasound frames in the input data set and with the grid-mapped cutoff radius (R). Using the statistics for the whole of the grid-mapped volume, a very strong linear correlation was shown to exist between the average number of data points used per grid point and the product of the number of frames with the cube of the cutoff radius (linear regression coefficient with 15 observations = 0.999998). On average, 66 values taken from various contributing ultrasound image frames were used to determine the value of a single voxel in the reconstructed data block. This situation is in contrast to the conventional 2-D image case with dependence on just a single value.

The percent CoV of the $1/r$ weighted values used in the reconstructions indicated the consistency of the distribution of values averaged during the grid-mapping procedure for every pixel in the reconstruction. In the example presented in Table 3, the average CoV taken over the whole plane was 0.23%.

Assessment of boundary continuity for a fixed segmentation level involved determining the width of the window needed to establish a continuous perimeter for the volume of interest (VOI). This relates directly to the ability to segment structures based on the grey-scale intensity values. The results in Table 3 corresponded to a

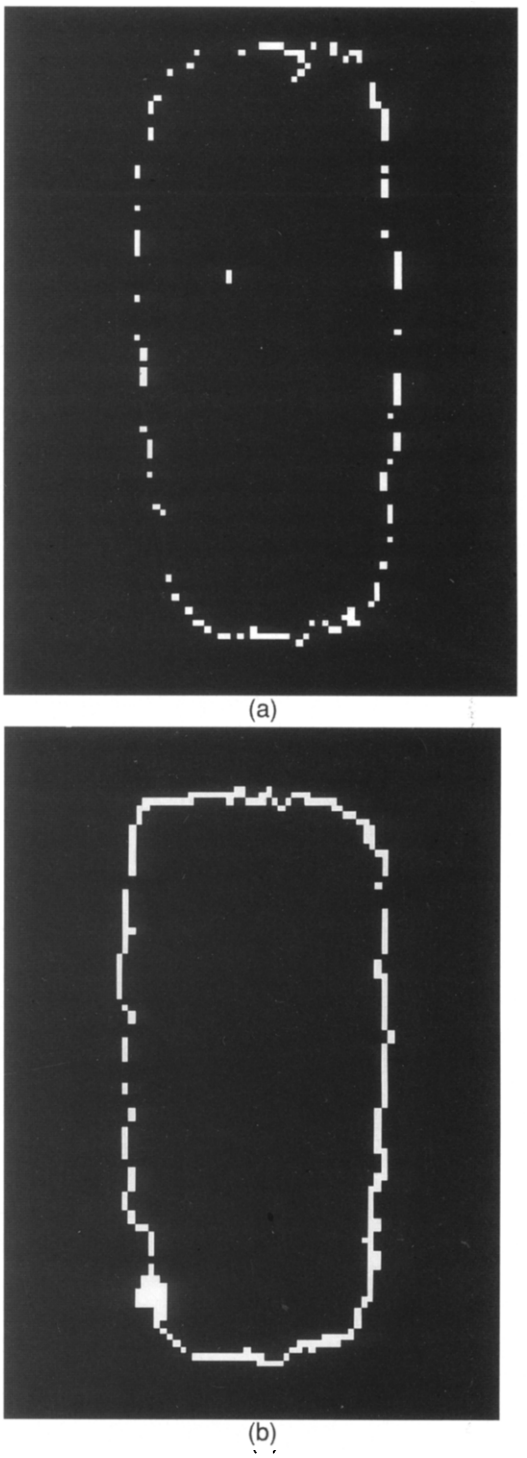

Fig. 4. Segmentation of pixels in the boundary of a foam phantom using a level of 40 and a window of 2. (a) The segmentable pixels in the original 2-D image. (b) The segmentable pixels in a compounded reconstructed plane identical in location.

"Level" setting of 40, the mean value of pixels in the reconstructed plane. The "Segmentation window width" then had to be set to ± 2.9 (15% of level) for the VOI in the reconstructed plane to obtain a qualitatively continuous and unbroken boundary. This compares well with a window width of ± 8.5 (42% of level) required for the same effect in the 2-D ultrasound image.

The more quantitative continuity measure of counting the number of pixels in the perimeter, detected by a standard setting of the Window parameter, demonstrated similar improvements, as follows.

A maximum pixel count of 345 for the perimeter of the VOI in Fig. 4 was obtained from a 1000-frame reconstruction, gridmapped using a limiting radius (R) of 0.5 mm, at a window of ± 2 (10% of level). In the typical reconstruction example (500 frames and R = 0.25 mm), using the same ± 2 (10% of level) window, 293 boundary pixels were detected (85% of the maximum) in the 3-D reconstructed plane compared to 121 (35% of maximum) in the original 2-D ultrasound image (Table 3). This 2- to 3-fold increase in boundary pixel count contributed directly to improvements seen both in the performance of statistical segmentation tools carrying out volumetric segmentation based on grey-scale intensity and structure boundaries, and in the 3-D depictions of reconstructed phantoms (Fig. 3).

The "Coherence Number" defined in Methods provided an abstract measure of ability to segment on grey-scale intensity that is independent of the tools to be used. The coherence number generated from the statistical analysis of the plane was found to correlate well with the qualitative assessment of image quality based on:

1. The ease and consistency of TOSCA segmentation;
2. The appearance of interfaces when revealed by displaying only pixels within a narrow range of values corresponding to an appropriate "level and window" selection;
3. The edge continuity of constituent interfaces using the "segmentation window width" measure. (Linear regression coefficient with 17 observations = 0.9737.)

In all cases, the grid-mapped 3-D reconstructions of "compounded" ultrasound data sets offered very significant improvement in interface coherence and the ability to segment structures of interest from grey-scale intensity.

Human carotid reconstructions in vivo

The human carotid reconstructions obtained are shown in Fig. 5a, b; they demonstrate the difference in geometry and, thus, pathology that can be detected in different individuals by this technique. Figure 6 shows the 2 extracted planes (XY and XZ) and demonstrates the benefit of having isotropic voxel reconstruction. This allows the data to be examined in the most clinically relevant planes without loss of resolution and without the usual anatomical restrictions.

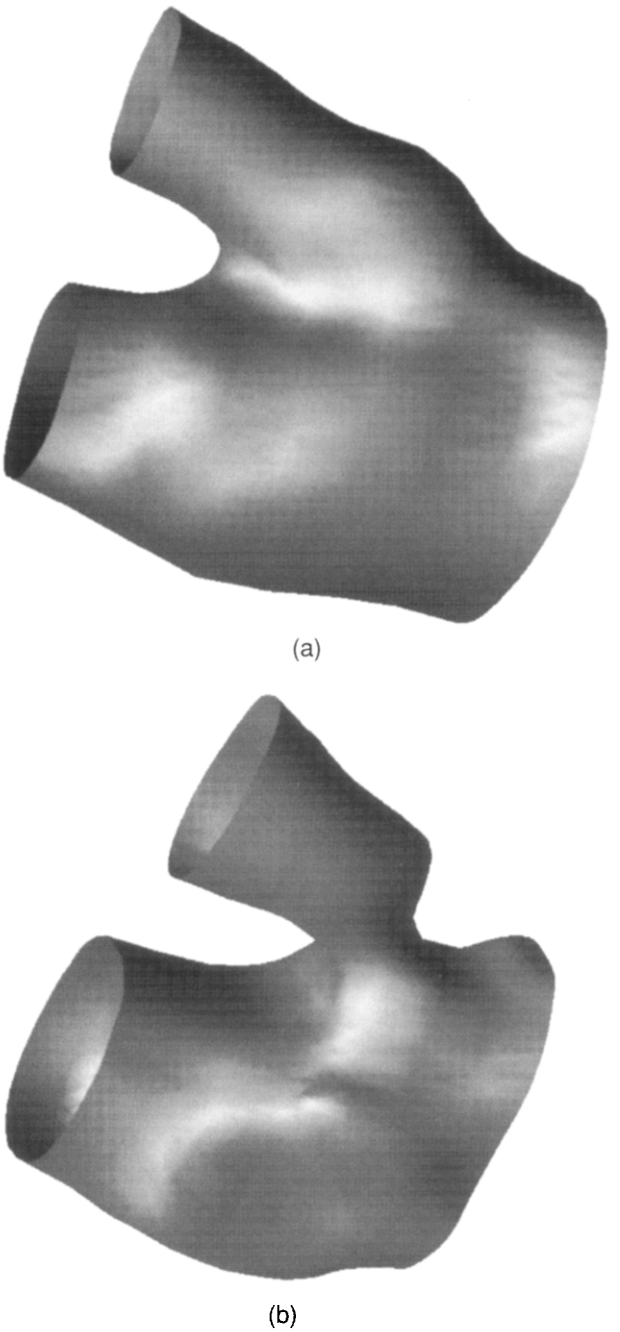

Fig. 5. Segmented and surface-rendered reconstructions of 2 examples of the biurification of the human carotid artery showing different geometries and pathologies.

DISCUSSION

The results presented support the assertion that data acquired using conventional 2-D ultrasound scanning

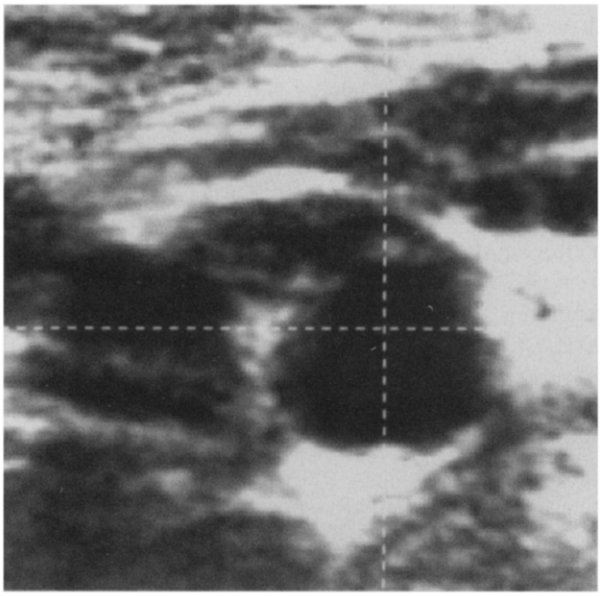

(a)

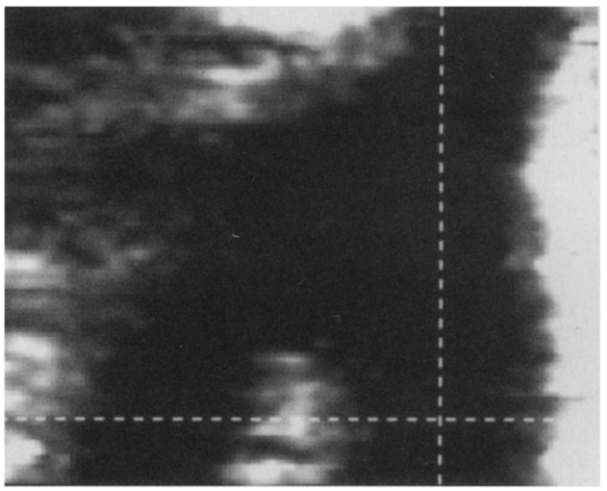

(b)

Fig. 6. Two planes (a) *XY* and (b) *XZ*, extracted from a 3-D carotid data set showing the benefit of isotropic voxel reconstruction and the ability to examine relevant planes free from anatomical restrictions and without loss of resolution. The dotted lines are the projections of a 3-D cross-wire and show the relative positioning of the orthogonal planes.

techniques can be reconstructed to provide high quality 3-D echo intensity images. These are capable of supporting reliable and consistent grey-scale structure segmentation and the accurate measurement (and progressive monitoring) of volume. The key points are as follows :

- The surface-rendered 3-D reconstruction of the foam-rubber phantom (Fig. 3) convincingly depicts not only details of the cylindrical body of the phantom (0.7 mL), but also the supporting wire (0.5 mm diameter);
- Tables 1 and 2 demonstrate the high degree of accuracy and reproducibility attained for volume measurements using water-filled balloon and cylindrical foam-rubber phantoms;
- The percent coefficients of variation show the distribution of $1/r$ weighted pixel values used in the 3-D reconstructions of the reference plane to be tightly grouped, with average values for the whole plane (13,000 pixels) of 0.25% for the 500-frame reconstruction (Table 3). The effective noise-to-signal figures are 1:400;
- The side-by-side comparison of a single 2-D ultrasound image frame and the echo intensities for the same plane, extracted from the 3-D reconstructed image of the foam-rubber phantom (Fig. 4), shows the differences in continuity of the interface obtained when a narrow range of pixel intensities is selected. Of the 345 pixels that might possibly be identified, the conventional 2-D image has only 35% of these and the plane from the 500-frame reconstruction has 87% (Table 3);
- The coherence numbers that characterise the ease and reliability of segmentation using the TOSCA level and window-type algorithm improve from 51 for the average of the "raw" 2-D image plane (13,000 pixels) to 190 for the 500-frame reconstruction (Table 3). This 370% improvement is an order of magnitude larger than that found when comparing coherence numbers for images before and after "smoothing" using a 2×2 box filter.

The power of the approach described originates in the freehand acquisition of extensive compounded data sets. First, the freehand aspect allows advantage to be taken of instinctive scanning behaviours and ensures a high density of data in the areas of greatest interest. Second, in association with the precision that can be achieved with extensive data sets and the Δ matrix formulation for 3-D registration of 2-D ultrasound images, the grid-mapping procedure described ensures that the echo intensity for each of the points in the 3-D reconstruction is calculated from a very significant number of observed data values. Third, compounding ensures an extensive positional sampling of echo intensities in the immediate neighbourhood of the reconstruction point and a range of insonation angles; this results in speckle reduction. The overall improvement in image quality allows reliable and accurate structure segmentation and volume assessment on the basis of grey-scale, 3-D reconstructed echo intensities without requiring the use of specialised, ultrasound-specific, algorithms. Finally, the format of the reconstruction allows advantage to be taken of the advanced 3-D analysis environments that once were exclusive to MRI and CT.

The ability to segment ultrasound data on the basis

of grey-scale intensities has to date been controversial. This has arisen from attempts to segment 2-D or 3-D ultrasound images that remain contaminated by speckle. The fact also remains that the grey-scale attributed to the same object might differ significantly between scanning instruments. In the present study, reliable automated grey-scale segmentation was only achieved after high-density sampling of compounded data was introduced and used in association with grid-mapping procedures. Reconstructions with the necessary level of coherence were then obtained that allowed standard statistical segmentation methods to succeed. IBM's TOSCA product provides for a profile of intensities to be obtained across a representative slice of the data block. This allows an appropriate level and window to be selected for the ROI and used for segmentation throughout the block. Reference features can then be used to provide cross-correlation of structures and their intensities between instruments and subsequent data sets. This has been checked using 3 ultrasound scanners and 2 calibrated 7.5 MHz linear array transducer/EPOS sensor configurations in various combinations.

An additional advantage of the methodology described is common to all 3-D imaging techniques and derives from the intrinsic limitations of 2-D data in volumetric analysis.

Although any 3-D image can be considered as a series of parallel 2-D plane images, volume assessments using 2-D data employ a relatively small number of independent planes. These are used to establish a set of 1-D or 2-D parameters to define a 3-D "model" and compute its volume (Fine, 1991; Gilja, 1994; Steen et al, 1994). The quality of the predicted volume will depend on the accuracy of the measurement of the parameters, the precision with which the planes selected meet the geometric requirements of the model, and the degree to which the structure "conforms" to the model. The major limitation lies with the "model" itself. Simple models make assumptions about the symmetry and regularity of structure. Even the more sophisticated, adaptive, modelling techniques that use training sets to select the most appropriate parametric model, become progressively less valid with increasing degrees of pathology (Cootes et al. 1994; Syn and Prager 1995).

The emphasis placed in our approach on acquiring overdetermined data sets to support the critical steps associated with 3-D registration and reconstruction is in marked contrast to what is described elsewhere. In the literature, regular parallel scanning techniques using a motor-driven linear transducer or specialised 2-D crystal arrays restricts the insonation angle to a single value. Fixed slice-intervals and physiological gating on acquisition limit the density of data points available for reconstruction. Where freehand scanning has been used, the subsequent 3-D reconstructions do not use a high density of compounded images in association with the grid-mapping approach. Instead, a relatively small number of approximately parallel, noncompounded, 2-D ultrasound image planes have been registered in 3-D and structure boundaries identified on these planes. These boundaries have then been used to produce a 3-D surface; the additional data points necessary to generate the surface triangles or polygons associated with standard surface-rendering techniques being provided by interpolation. Alternatively, 3-D shape modelling has been used with constraints provided by the structure boundaries established on the various registered 2-D image planes. Although, in general, the appearance of such surface-rendered objects will be good, the reliance on relatively low data densities and single insonation angle must restrict the precision associated with such segmentation and volume assessments.

In contrast, the methodology described in this paper avoids the problems associated with reliance on limited data or on volume measurement from potentially inaccurate model-fitting by direct assessment of volume based on segmentation of the 3-D reconstructed images.

The 3-D reconstruction techniques described are not restricted to use with linear array transducers and can, in principle, be applied wherever 2-D ultrasound is used. Reconstruction of data acquired with other probe types has been achieved in our laboratory. Extension of the system to address *in vivo* studies in a research or clinical environment requires the physiological monitoring of functions that produce relative motion or distortion of the structures of interest. The facility to select those 2-D ultrasound images captured under identical cardiac cycle conditions has been described. Extension to handle respiratory motion is being developed. The second stereo channel of the S-VHS tape is used to record such information. Provided that the selection criteria are sufficient to "freeze" effectively the associated motion, a consistent 3-D reconstruction can then be obtained. This has already been demonstrated in this laboratory through 3-D reconstruction of *in vivo* vascular structures using only the 2-D ultrasound images recorded close to the midpoint of diastole (Allott et al. 1996).

Using the equipment described, a 3-D reconstruction is available for segmentation and analysis within 30 min from acquisition of the 2-D ultrasound images. Of this time, the "interactive, real-time" aspects of the process take less than 10 min. The bulk of the time is taken up by tasks that can run unattended once initiated; moreover, this batch processing time can be reduced by up to a factor of 3 using the faster hardware now available at a similar system cost. These overall timings are believed to be compatible with routine use in a clinical diagnostic environment and for clinical and preclinical studies (Hal-

liwell and Woodcock, personal communications). In this laboratory in excess of 2000 3-D reconstructions of ultrasound data sets, from both *in vitro* and *in vivo* sources, have been made with this system in the past 12 months, demonstrating the potential to provide 3-D images of clinical relevance. Reconstructions of the bifurcation of human carotid arteries demonstrate the benefit of having isotropic voxel reconstruction, allowing the data to be examined in the most relevant planes without loss of resolution and free from anatomical restrictions.

SUMMARY

This paper has presented results that support the following assertions:

1. Accurate 3-D reconstruction from compound, freehand, ultrasound images has been achieved.
2. Compounding of 2-D images and generation of a regular 3-D data block leads to better image structure coherence, so that the 3-D reconstructions are comparable with CT and MRI images and formatted appropriately for use with state-of-the-art 3-D Medical Image Analysis products.
3. Provided that EPOS data and system scaling factors can be obtained with the required accuracy, any ultrasound image data set, from any 2-D transducer type or anatomical location, could be reconstructed in 3-D by these methods.
4. The accuracy and precision of 3-D reconstruction and volume measurement from these compounded images is sufficient for clinical utility in patient monitoring.
5. The computation processes involved in 3-D spatial orientation and generation of a regular 3-D data block from ultrasound images no longer present a bottleneck in data processing. Reconstruction and segmentation of a data set can be achieved in times appropriate for clinical utility.

We have described the process of 3-D reconstruction and accurate volume measurement, starting with data acquired using conventional 2-D ultrasound scanning techniques. These procedures, together with readily available commercial software and equipment, produce a system that is capable of delivering sufficiently significant benefits to propose its use in the clinical environment.

REFERENCES

Allott CP, Arundel PA, Barry CD, et al. Freehand, quantitative 3-D ultrasound imaging and its application (abstr). Eur J Ultrasound 1996;3(Suppl):S9.

Cootes TF, Hill A, Taylor CJ, Haslem J. The use of active shape models for locating structures in medical images. Image Vision Computing 1994;12:276–285.

Detmer PR, Bashein G, Hodges T, Beach KW, Strandness DE Jr. 3D ultrasonic image feature location based on magnetic scan head tracking: In vitro calibration and validation. Ultrasound Med Biol 1994;20:923–936.

Elliot PJ, Diedrichsen J, Goodson K, Riste-Smith R, Sivewright GJ. An object oriented system for 3D medical image analysis. IBM Syst J 1996;35:1–18.

Fine D. Three-dimensional ultrasound imaging of the gallbladder and dilated biliary tree: reconstruction from real-time B-scans. Br J Radiol 1991;64:1056–1057.

Franceschi D, Bondi J, Rubin JR. A new approach for three-dimensional reconstruction of arterial ultrasonography. J Vasc Surg 1992; 15:800–805.

Gardener JE, Lees WR, Gillams A. Volume imaging with ultrasound. Radiology 1991;181(P):133.

Geiser EA, Ariet M, Conetta DA, Lupkiewcz SM, Christie LG. Dynamic three-dimensional echocardiographic reconstruction of the intact human left ventricle; Technique and initial observations in patients. Am Heart J 1982;103:1056–1065.

Gilja OH. In vitro evaluation of three-dimensional ultrasonography in volume estimation of abdominal organs. Ultrasound Med Biol 1994:20:157–165.

Hamper UM, Trapanotto V, Sheth S, Dejong MR, Caskey CI. Three-dimensional US preliminary clinical experience. Radiology 1994; 191:397–401.

Hell B. 3D Sonography. Int J Oral Maxillofac Surg 1995;24:84–89.

Hernandez A, Basset O, Chirossel P, Gimenez G. Spatial compounding in ultrasound imaging using an articulated scan arm. Ultrasound Med Biol 1996;22:229–238.

Howry DH, Posakony G, Cushman R, Holmes JH. Three dimensional and stereoscopic observation of body structures by ultrasound. J Appl Physiol 1956;9:304–306.

Hughes SW, D'Arcy TJ, Maxwell DJ, et al. Volume estimation from multiplanar 2-D ultrasound images using a remote electromagnetic position and orientation sensor. Ultrasound Med Biol 1996;22:561–572.

Kelly IM, Gardener JE, Brett AD, Richards R, Lees WR. Three-dimensional US of the fetus - work in progress. Radiology 1994; 192:253–259.

King DL, King DL Jr, Yi-Ci Shao M. Three-dimensional spatial registration and interactive display of position and orientation of real-time ultrasound images. J Ultrasound Med 1990;9:525–532.

Kok-Hwee Ng, Evans JL, Vonesh MJ, Meyers SN, Mills TA. Arterial imaging with a new forward-viewing intravascular ultrasound catheter. II. Three-dimensional reconstruction and display of data. Circulation 1994;89:718–723.

Levine RA, Weyman AE, Handschumaker MD. Three-dimensional echocardiography: Techniques and applications. Am J Cardiol 1992;69:121H–130H.

Mintz GS, Keller MB, Fay FG. Motorised IVUS transducer pull-back permits accurate quantitative axial measurements (abstr). Circulation 1992;86-I:323s.

Moritz WE, Medema DK, Ainsworth M, McCabe D, Pearlman AS. Three-dimensional reconstruction and volume calculation from a series of nonparallel, real-time, ultrasonic images. Circulation 1980;62(Suppl);111–143.

Moskalik A, Carson PL, Meyer CR, et al. Registration of three-dimensional compound ultrasound scans of the breast for refraction and motion corrections. Ultrasound Med Biol 1995;21:769–778.

Nelson TR, Pretorius DH, Slansky M, Hagen-Ansert S. Three-dimensional echocardiographic evaluation of fetal heart anatomy and function. J Ultrasound Med 1996;15:1–9.

Picano E, Landini L, Distante A, Salvadori M, Lattanzi F. Angle dependence of ultrasonic backscatter in arterial tissues; a study *in vitro*. Circulation 1985;72:573–576.

Rankin RN, Fenster A, Downey DB, et al. Three-dimensional sonographic reconstruction: Techniques and diagnostic applications. AJR 1993;161:695–702.

Riccabona M, Nelson TR, Pretorius DH, Davidson TE. Distance and volume measurement using three-dimensional ultrasonography. J Ultrasound Med 1995;14:881–886.

Rosenfield K, Losordo DW, Ramaswamy K, Isner JM. Three-dimensional reconstruction of human coronary and peripheral arteries from images recorded during two-dimensional intravascular ultrasound examination. Circulation 1991;84:1938–1956.

Schumacher DA. Fast anamorphic image scaling. In: Arvo J, ed. Graphics gems II. London: Academic Press, 1991:78–79.

Shattuck DP, von Ramm OT. Compound scanning with a phased array. Ultrason Imaging 1982;4:93–107.

Sivewright GJ, Elliot PJ. Interactive region and volume growing for segmenting volumes in MR and CT images. Med Inf 1994;19:71–80.

Steen E, Olstad B. Volume rendering of 3D medical ultrasound data using direct feature mapping. IEEE Trans Med Imag 1994;13:517–525.

Syn M, Prager RA. Model based approach to three-dimensional ultrasound imaging. In: Bizais Y, Barillot C, Di Paola R, eds. Information processing in medical imaging: Computer imaging and vision. London: Kluwer Academic, 1995:361–362.

Vogel M, Ho SY, Buhlmeyer K, Anderson RH. Assessment of congenital heart defects by dynamic three-dimensional echocardiography; methods of data acquisition and clinical potential. Acta Paediatr Suppl 1995;410:34–39.

von Birgelen C, Slager CJ, Di Mario C, de Feyter PJ, Serruys PW. Volumetric intracoronary ultrasound; A new maximum confidence approach for the quantitative assessment of progression-regression of atherosclerosis? Atherosclerosis 1995;118(Suppl):S103–S113.

von Ramm OT, Durham NC, Smith SW, Carroll BA. Real time volumetric US imaging. Radiology 1994;193(P):308.

Zosmer N, Jurkovic D, Jauniaux E, Gruboeck K, Lees C. Selection and identification of standard cardiac views from three-dimensional volume scans of the fetal thorax. J Ultrasound Med 1996;15:25–32.